J. Membrane Biol. 84, 239–248 (1985)

The Journal of
Membrane Biology

Transepithelial Transport of Nonelectrolytes in the Rabbit Mandibular Salivary Gland

R.M. Case, D.I. Cook*, M. Hunter, M.C. Steward, and J. A. Young*
Department of Physiology, University of Manchester, Manchester, M13 9PT, United Kingdom

Summary. The characteristics of nonelectrolyte secretion by the rabbit mandibular salivary gland have been investigated in an *in vitro*, perfused preparation. The concentrations of ^{14}C-labeled nonelectrolytes were measured in saliva samples collected over a range of flow rates during the secretory response of the gland to continuous acetylcholine infusion. Of the nine nonelectrolytes studied, the two particularly lipid-soluble molecules, ethanol and antipyrine, appeared in the saliva at approximately the same concentration as in the perfusate, regardless of the secretory flow rate. The more polar molecules (urea, ethanediol, thiourea, glycerol, erythritol, mannitol and sucrose) appeared at saliva/perfusate concentration ratios (ϕ) which showed a strong dependence on flow. With the exception of thiourea, this could be attributed to the combined contributions of diffusion and solvent drag.

For the polar nonelectrolytes, estimates have been obtained of both the permeability coefficients of the gland (P) and the solvent-drag filtration coefficients ($1 - \sigma$). The relation between $1 - \sigma$ and molecular radius suggests that small polar nonelectrolytes and the bulk of the secreted water cross the epithelium via aqueous channels that are approximately 0.8 nm in width. The location of the channels remains uncertain because tissue space measurements indicate that the nonelectrolytes most affected by solvent drag have access to both transcellular and paracellular pathways.

Key words salivary glands · nonelectrolytes · solvent drag · diffusion

Introduction

In the last few years, the mechanisms whereby solutes and water cross epithelia have come under close scrutiny, but whether the bulk of transepithelial fluid transport takes place via para- or transcellular routes and the extent to which solute concentration profiles, built up in the basolateral interstices of the transporting epithelial cells, may influence overall transport, remain matters of great controversy. Reasons of experimental convenience have dictated that the greatest number of investigations of transepithelial fluid transport have been performed on absorbing epithelia such as kidney tubules, gallbladder, and small intestine and, although studies on secretory tissues such as gastric glands, choroid plexus and insect buccal (salivary) glands are available, few have been published on the fluid-secretory mechanisms and pathways of the major compound exocrine glands. By studying the excretion of small nonelectrolytes by the rabbit mandibular gland, we hoped to gain some general insight into the mechanisms of exocrine fluid secretion.

Our findings indicate that the gland handles small, relatively lipophilic molecules (ethanol and antipyrine) differently from more hydrophilic molecules of comparable size (urea, ethanediol, glycerol, erythritol, mannitol and sucrose). For the latter group, we have interpreted the data in terms of two separate passive mechanisms for solute entry into the saliva, one involving simple molecular diffusion, and the other involving convective solute flow (solvent drag). For the former group, it is evident that solute permeation is rapid and complete, indicating that the solutes can cross lipid membranes directly and bypass the aqueous channels through which the nonlipophilic molecules seem to pass. In analyzing our results, we have also examined the extent to which the presence of unstirred layers, leading to the development of solute concentration profiles in the basolateral labyrinth of the epithelium, may have invalidated or distorted our interpretation, and an analysis of this problem is presented in an appendix.

A preliminary report of some aspects of this work has previously been published (Case et al., 1983).

* *Present Address*: Department of Physiology (F13), University of Sydney, N.S.W. 2006, Australia.

Table 1. Some relevant physical properties of the nonelectrolyte tracers used in the study

Nonelectrolyte	Molecular weight[a] M	Diffusion coefficient[b] (10^{-6} cm^2 sec^{-1}) D_o	Hydrodynamic radius[c] (nm) a	Oil/water partition[d] (10^{-3}) K
Ethanol	46	14.2	0.21	32.0
Urea	60	12.4	0.23	0.15
Ethanediol	62	12.2	0.24	0.49
Thiourea	76	11.0	0.26	1.20
Glycerol	92	10.0	0.28	0.07
Erythritol	122	8.7	0.32	0.03
Mannitol	182	7.1	0.38	0.0012
Antipyrine	188	7.0	0.39	32.0
Sucrose	342	5.2	0.51	0.001
Inulin[e]	5200	1.3	—	—

[a] The molecular weights have not been adjusted to allow for the ^{14}C label.
[b] The free solution diffusion coefficients (D_o) have been calculated from the molecular weights (M), taking the published value for sucrose of 5.2×10^{-6} cm^2 sec^{-1} measured at 25°C (Longsworth, 1953) as a reference, by using the following formula: $D_o \cdot M^{1/2}$ = constant (Stein, 1967).
[c] The Stokes-Einstein radii (a_{se}) have been calculated from the formula $D_o \cdot a_{se}$ = constant, using the published value for sucrose of 0.46 nm as a reference, and are corrected for deviations due to small molecular size by the formula: $a = [a_{se} + \sqrt{a_{se}^2 + 0.2a_{se}}]/2$ (Schultz & Solomon, 1961).
[d] Oil/water partition coefficients from Collander (1954), Wright and Diamond (1969) and Wright and Pietras (1974).
[e] The molecular weight of inulin is only approximate. The value quoted for the diffusion coefficient is from Phelps (1965). The molecule is elongated in shape and has semi-axes of 2.5 and 0.11 nm (Middleton, 1977).

Materials and Methods

Male half-lop albino rabbits, weighing 1.3 to 3.0 kg, fed a normal maintenance diet (B.P. Nutrition), were used in all experiments. They were anesthetized with urethane dissolved in physiological saline (30 g/dl) administered intraperitoneally (5 ml/kg body weight), with subsequent intravenous supplements as required. A tracheostomy was established and the mandibular glands exposed, excised and transferred to an organ bath (37°C) as described in detail previously (Case et al., 1980).

Glands were perfused intravascularly at 4 ml/min with the aid of a constant-flow peristaltic perfusion pump. The perfusion fluid, which was equilibrated with 5% CO_2 in O_2 to maintain a constant pH of 7.4, contained (in mmol/liter): Na = 146.0, K = 4.5, Ca = 1.5, Mg = 1.0, Cl = 128.5, HCO_3 = 25.0, SO_4 = 1.0, PO_4 = 1.0 and glucose = 5.0 (osmolality, determined from the freezing point, was 283 mosmol/kg H_2O). In each experiment, a ^{14}C-labeled nonelectrolyte was added to the perfusion fluid in a tracer concentration. The maximum nonelectrolyte concentration employed was 0.11 μmol/liter and the minimum isotope activity was 11 μCi/liter. The nonelectrolytes used, together with their relevant physical characteristics, are listed in Table 1.

Salivary secretion was evoked by continuous infusion of acetylcholine chloride into the perfusion line, remote from the gland and proximal to the perfusion pump, giving a final agonist concentration of 0.8 μmol/liter. The α- and β-adrenergic antagonists, phentolamine and propranolol, were included routinely in the perfusate in concentrations of 2.5 μmol/liter, so as to avoid complications arising from spontaneous or evoked release of catecholamines from intraglandular sympathetic nerve endings.

Glands were perfused with fluid containing labeled nonelectrolytes for 15 min before acetylcholine infusion was begun; during this time little or no saliva was secreted. After the onset of acetylcholine stimulation, saliva was collected over timed intervals into tared polycarbonate vessels which were immediately stoppered, reweighed and stored at 4°C pending analysis. Sample collection followed a standard protocol: first, five samples were collected over consecutive 1-min periods, after which one 2-min and one 3-min sample, and then up to nine additional 5-min samples were collected. The collection times were chosen so as to give samples of approximately equal volume. In order to eliminate catheter and duct dead-space effects, the sample collected during the first minute after the onset of stimulation was discarded. Since, at low secretory rates, ductal water absorption becomes significant (Young & van Lennep, 1979) and would therefore alter the nonelectrolyte concentrations appreciably, we terminated the experiment when the flow rate fell below 25 μl/min (i.e. 10% of the maximum).

Activities of ^{14}C in saliva and perfusate were determined with a Packard Tri-Carb 460c liquid scintillation spectrometer, using 25-μl samples of saliva or perfusate dispersed in 4 ml of PCS scintillation fluid (Amersham International, U.K.).

To assess the extent to which the various nonelectrolytes employed in this study could cross the plasma membrane and enter the cytosol of the secretory cells, we performed a series of space-determination experiments on incubated gland slices. Glands were removed from anesthetized rabbits and chopped into slices about 800 μm thick with the aid of a McIlwain automatic tissue chopper. The slices were then transferred to glass vials containing 10 ml of perfusate and gassed with 5% CO_2 in O_2 at 37°C in a shaking water-bath. Following 10 to 20 min of preincubation, the slices were transferred to fresh vials containing 10 ml of perfusate plus radio-labeled nonelectrolytes and acetylcholine in the same activities and concentrations as employed in the perfusion experiments. The slices were removed after various incubation periods, blotted gently on moistened filter paper, and

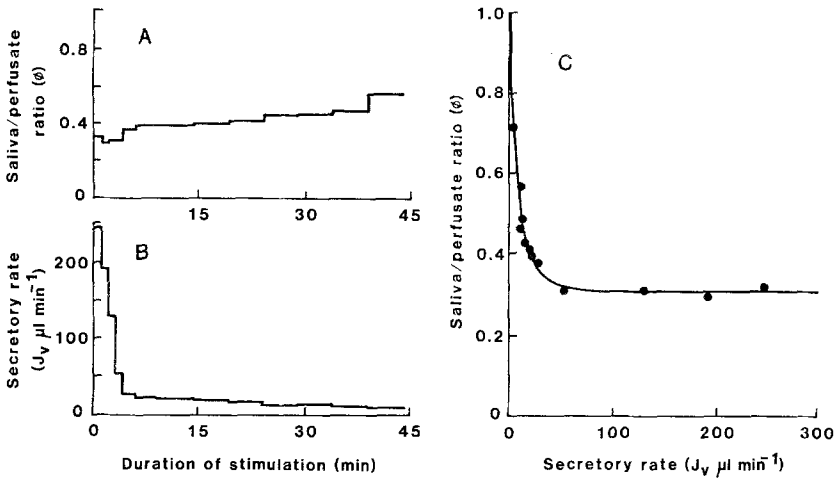

Fig. 1. Data from a representative experiment in which ^{14}C-urea was included in the perfusate. *A*. Saliva/perfusate concentration ratios (ϕ) of consecutive saliva samples plotted against time over the first 45 min of acetylcholine stimulation. *B*. Secretory volume flow (J_v) over the same period. *C*. Saliva/perfusate ratios plotted against flow using the data of *A* and *B*. The curve, which was fitted by a least-squares method, has the form of Eq. (3) with P = 6.0 mm^3 min^{-1} and $1 - \sigma = 0.30$

transferred to tared vials which were immediately stoppered and reweighed. After addition of 500 µl of distilled water, the slices were disintegrated by sonication for 30 sec. Radioactivity was then determined by liquid scintillation spectrometry as described above and the volume of distribution of each nonelectrolyte was estimated by reference to the activity of the labeled compound in the incubation medium and expressed in ml per g wet tissue weight.

Acetylcholine chloride and propranolol hydrochloride were obtained from Sigma Chemical Company and phentolamine mesylate from Ciba-Geigy Ltd. All radioisotopes were obtained fresh from Amersham International (Amersham, U.K.) or New England Nuclear (Dreieich, F.R.G.).

Data Analysis

The activities of the nonelectrolytes in the saliva samples were expressed as fractions ϕ of the corresponding activities in the gland perfusate, and plotted as a function of the salivary secretory rate J_v. Initially, the data were analyzed in terms of the Kedem and Katchalsky (1958) solute flux equation (Case et al., 1983). However, this equation is strictly only applicable to a single thin membrane. Subsequently, therefore, we preferred to use the differential form of the Kedem-Katchalsky equation, integrated across the finite thickness of a more complex barrier (Patlak et al., 1963).

If, for example, the barrier extends from $x = 0$ to $x = \delta$, and positive flux is in the direction of increasing x, then the solute flux, J_n (mol cm^{-2} sec^{-1}), is given at any point by:

$$J_n = -\omega' RT \frac{dC}{dx} + (1 - \sigma) C J_v \tag{1}$$

where $\omega' RT$ is a form of solute permeability coefficient (cm^2 sec^{-1}), σ the reflection coefficient, J_v the volume flux (cm^3 cm^{-2} sec^{-1}) and C the solute concentration (mol cm^{-3}) at x. Integrating from $x = 0$ to $x = \delta$, and applying the boundary condition that at $x = 0$, C is equal to the perfusate concentration C^P, and that at $x = \delta$, C is equal to the saliva concentration C^S, we obtain the following expression for solute flux:

$$J_n = (1 - \sigma) \cdot J_v \cdot \frac{C^S - C^P \cdot \exp(Q\delta)}{1 - \exp(Q\delta)} \tag{2}$$

where $Q = (1 - \sigma) J_v / \omega' RT$.

In a unilateral (secreting) system, $C^S = J_n / J_v$. Consequently, using ϕ to represent C^S/C^P and P for $\omega' RT/\delta$, Eq. (2) may be rearranged as:

$$\phi = \frac{1 - \sigma}{1 - \sigma \exp(-J_v(1 - \sigma)/P)}. \tag{3}$$

When $J_v = 0$, then $\phi = 1$ and, as $J_v \to \infty$, then $\phi \to (1 - \sigma)$.

This equation has the form of a rectangular hyperbola with a vertical intercept of $\phi = 1$ at $J_v = 0$ and a horizontal asymptote of $1 - \sigma$. From experimentally determined values for ϕ and J_v, we may obtain estimates of P and $1 - \sigma$ by fitting Eq. (3) to the data. To do this, we have developed our own least-squares optimization routine based on the Gauss-Newton method.

Since Eq. (3) is nonlinear, in order to draw a mean curve of best fit for each nonelectrolyte, we used the means of the P and $1 - \sigma$ values obtained with our search routine from individual experiments. Confidence limits for the mean curve, $var(\phi)$, are constructed from the variances of P, $var(P)$, and σ, $var(\sigma)$, and their covariance, $cov(P, \sigma)$, using the following formula which is derived from a Taylor expansion of Eq. (3) using the principles outlined by Cornish-Bowden (1976):

$$var(\phi) = \left(\frac{\partial \phi}{\partial \sigma}\right)^2 \cdot var(\sigma) + 2 \cdot \frac{\partial \phi}{\partial \sigma} \cdot \frac{\partial \phi}{\partial P} \cdot cov(P, \sigma) + \left(\frac{\partial \phi}{\partial P}\right)^2 \cdot var(P). \tag{4}$$

Results

The isolated rabbit mandibular gland secretes little or not at all when perfused in the absence of an appropriate secreto-motor agonist but when, for instance, it is stimulated by the continuous infusion of acetylcholine in optimal doses (0.8 µmol/liter), an initially large secretory response is evoked which declines over about 30 min to attain a steady value (Case et al., 1980). In the present experiments, the initial secretory rate in 54 experiments averaged 201.7 µl/min ± 67.8 SD over the second minute of stimulation, and had fallen to 33.1 µl/min ± 12.7 SD after 30 min and to 29.8 µl/min ± 11.8 SD after 45 min. These values are normal for this degree of acetylcholine stimulation (*cf.* Case et al., 1980). The flow response in a typical experiment is shown in Fig. 1*B*.

When the activities of each nonelectrolyte in the saliva, expressed as a fraction (ϕ) of the perfusate activity, were plotted as a function of salivary secretory rate (J_v), the results fell into three distinct groups (Figs. 2, 3 and 4). The first, and largest group, comprised urea, ethanediol, glycerol, erythritol, mannitol and sucrose (Figs. 2 and 3). In the case of these solutes, the plot of ϕ against J_v had the form of a rectangular hyperbola, tending to high values of ϕ (approaching 1.0) at low rates, and falling rapidly to approach a horizontal asymptote, substantially lower than 1.0, at high flow rates. The results of a typical experiment (with urea) are shown in Fig. 1 where, in addition to the plot of ϕ against J_v, plots of ϕ and J_v as functions of the duration of the experiment are shown. For each experiment of this type, Eq. (3) was fitted to the data in order to obtain values for P, the gland permeability coefficient, and $1 - \sigma$, the filtration coefficient. The mean values for P and $1 - \sigma$ for each nonelectrolyte in the group are shown in Table 2. From the data shown in Table 2, best-fit curves as described by Eq. (3) were fitted to the pooled data as shown in Figs. 2 and 3, together with 95% confidence limits obtained from Eq. (4).

The second group (Fig. 4) comprised the two relatively lipid-soluble compounds, ethanol and antipyrine. For both compounds the value of ϕ was always close to 1.0 and showed only slight flow dependence. For antipyrine, ϕ averaged 0.968 ± 0.005 SEM (n = 23) above a flow rate of 60 μl/min but, at lower flow rates, it rose slightly, averaging 1.019 ± 0.004 (n = 52) at a mean flow rate of 36 μl/min. This rise probably reflects ductal water reabsorption which becomes more significant at low secretory rates. For ethanol, the corresponding mean values of ϕ were 0.955 ± 0.012 (n = 21) above 60 μl/min and 0.901 ± 0.009 (n = 52) below 60 μl/min, i.e. as flow declined, ϕ fell slightly below unity for ethanol but rose above unity for antipyrine. The fall was probably due to evaporation of the volatile ethanol from the saliva drop which hangs on the collection catheter for prolonged periods when flow is low.

A third pattern was seen in the case of thiourea (Fig. 4C). For this compound, ϕ was relatively high, averaging 0.533 ± 0.011 (n = 123), and showed no clear-cut flow dependence, although in many experiments the value of ϕ fell slightly around a flow rate of 50 μl/min only to rise again at lower

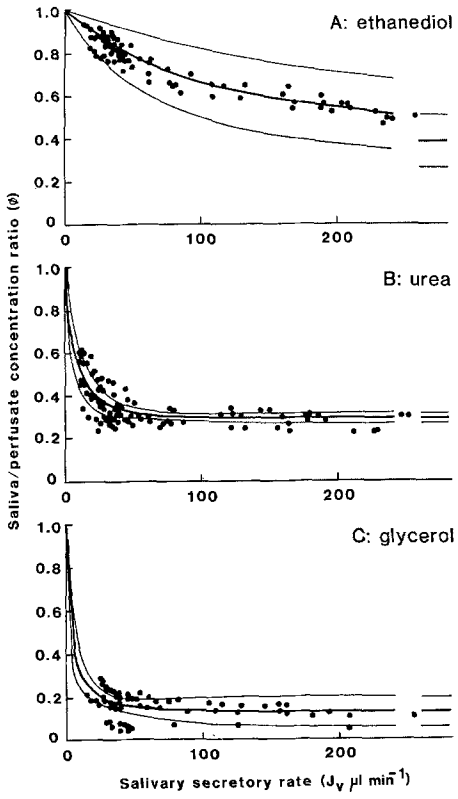

Fig. 2. Dependence of the saliva/perfusate concentration ratio on the secretory flow rate for: *A*. ethanediol, *B*. urea, *C*. glycerol. In each case, pooled data from all the experiments are shown, together with a curve of the form of Eq. (3) based on average estimates of P and $1 - \sigma$ (Table 2). Also shown are the 95% confidence limits of the curve [Eq. (4)] and, at the far right, the horizontal asymptote and its confidence limits

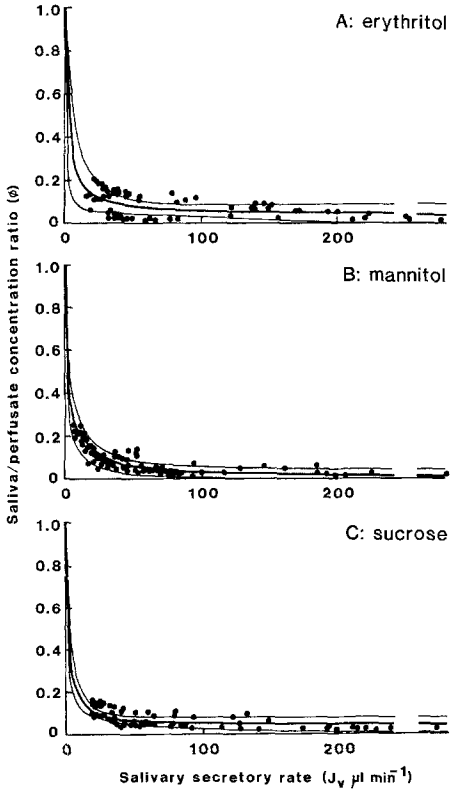

Fig. 3. Pooled data with mean curves of best fit and confidence limits (as in Fig. 2) for: *A*. erythritol, *B*. mannitol, *C*. sucrose

flow rates. We did not attempt to fit Eq. (3) to these data.

In Table 3 are summarized the results of experiments in which the volumes of distribution of various nonelectrolytes were studied in slices of gland tissue incubated for various periods of up to 2 hr in perfusate containing labeled nonelectrolytes. Equilibration throughout the available space was rapid, and virtually complete after 20 min of incubation, except in the case of erythritol. Sucrose and inulin occupied about 40% of the total tissue water, whereas thiourea, urea, ethanol, ethanediol and antipyrine appeared to occupy the entire tissue space. Since erythritol equilibration was incomplete even after 2 hr incubation, we cannot say what its ultimate volume of distribution would have been. It appears to have occupied the extracellular space quite rapidly and then slowly to have permeated the intracellular compartment as well.

Table 2. Estimates of P, the permeability coefficient, and $1 - \sigma$, the filtration coefficient, for six small polar nonelectrolytes[a]

	$k_{oil}/M^{1/2} \times 10^6$	P^b	$1 - \sigma$	n
Ethanediol	62.2	99.43 ± 18.57	0.391 ± 0.039	5
Urea	19.4	6.54 ± 1.37	0.294 ± 0.008	7
Glycerol	7.3	3.21 ± 0.72	0.136 ± 0.022	5
Erythritol	2.7	2.55 ± 0.83	0.048 ± 0.016	5
Mannitol	0.09	2.66 ± 0.42	0.012 ± 0.015	6
Sucrose	0.05	1.75 ± 0.30	0.045 ± 0.013	6

[a] Values are means ± SEM; n indicates number of glands studied. $k_{oil}/M^{1/2}$ is the ratio of the partition coefficient to the square root of the molecular weight (*see* Table 1).

[b] The units of P are $mm^3\ min^{-1}$ since the permeability coefficient does not take into account the surface area of the secretory epithelium.

Discussion

Previous studies of nonelectrolyte secretion by exocrine glands have revealed important differences between the behavior of lipid-soluble molecules and small polar molecules (Burgen, 1956; Burgen & Emmelin, 1961; Mangos & McSherry, 1970; Mangos et

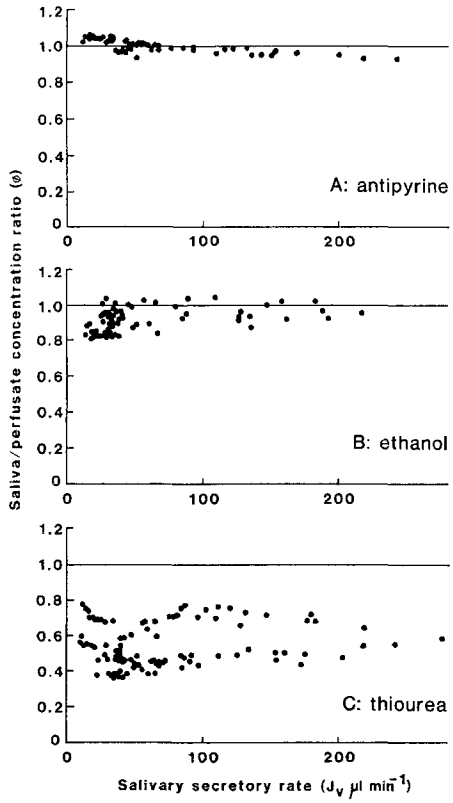

Fig. 4. Pooled data for: *A.* antipyrine, *B.* ethanol, *C.* thiourea. The horizontal line represents a saliva/perfusate ratio of 1.0

Table 3. Tissue space occupied by various nonelectrolytes[a]

	Duration of incubation (min)				n
	5	20	60	120	
Ethanol[b]	0.826 ± 0.159	0.917 ± 0.115	0.831 ± 0.106	0.965 ± 0.222	3
Urea[b]	0.631 ± 0.121	0.910 ± 0.059	0.916 ± 0.020	0.979 ± 0.042	3
Ethanediol[b]	0.911 ± 0.118	0.986 ± 0.099	0.990 ± 0.064	0.964 ± 0.054	4
Thiourea[b]	0.527 ± 0.088	0.892 ± 0.147	0.806 ± 0.134	0.966 ± 0.186	3
Erythritol	0.467 ± 0.187	0.451 ± 0.016	0.752 ± 0.124	0.799 ± 0.143	3
Antipyrine[b]	0.656 ± 0.134	0.913 ± 0.118	1.146 ± 0.107	1.089 ± 0.153	6
Sucrose	0.281 ± 0.033	0.307 ± 0.037	0.327 ± 0.017	0.348 ± 0.057	6
Inulin	0.422 ± 0.048	0.376 ± 0.024	0.480 ± 0.035	0.444 ± 0.032	6

[a] Values are means ± SEM (n = number of observations), expressed as the volume of distribution (ml) per g wet tissue mass.

[b] Analysis of variance showed that the volume of distribution of these five compounds did not differ significantly among themselves ($P > 0.05$). The pooled mean volume for these compounds at 120 min was 1.01 ml/g ± 0.06 (n = 19).

al., 1973; Takai et al., 1983). Burgen (1956), on the basis of flow-dependence studies with the dog parotid gland, suggested that there might exist two distinct but parallel transepithelial pathways for nonelectrolyte secretion, one permeable to molecules according to their lipid solubility and the other permeable to small polar molecules according to their molecular radius.

Our studies support the idea that, irrespective of size, molecules of high lipid solubility such as ethanol and antipyrine appear in the saliva at concentrations close to the perfusate concentration regardless of secretory rate. This pattern has been reported previously for antipyrine in some preliminary studies by Welch et al., (1975). The excretory pattern for polar molecules, however, differs in that, although the salivary concentration approaches the perfusate concentration at low secretory rates, it falls to a finite plateau value at higher rates. (We did not, incidentally, observe the rise in concentration with flow reported by Burgen (1965) but this may reflect the different methods of stimulation used in the two studies. Burgen varied the frequency of electrical stimulation of the auriculotemporal nerve in order to evoke secretion at different rates, and this would almost certainly have exposed the secretory cells to varying concentrations of acetylcholine. Our study was conducted with a constant acetylcholine concentration, and we have reason to believe that epithelial "permeability" rises with increasing acetylcholine concentration (Potter et al., 1984).)

The main purpose of our study was to examine the permeation mechanism of the small polar nonelectrolytes. If we exclude the possibility of active transport (thiourea may be an exception: *see below*), the only ways by which nonelectrolytes can move from interstitium to saliva are by simple diffusion and solvent drag. Since the saliva/perfusate concentration ratio of all the polar nonelectrolytes studied remained above zero and approached a plateau as salivary flow increased, it would appear that solvent drag contributed to net secretion in each case, even for sucrose. (An alternative explanation, *viz.* pseudo solvent drag, is considered below.) It would therefore seem appropriate to use Eq. (3) to fit the data, although the values of P and $1 - \sigma$ thus obtained may be composites of two or more independent values, if, for example, both transcellular and paracellular permeation pathways exist.

Comparison of the values of P and $1 - \sigma$ listed in Table 2 with the physical properties of the molecules (Table 1), particularly the ratio of the oil/water partition coefficient to the square root of the molecular weight (Table 2), shows an obvious correlation with lipid solubility and molecular size, in accordance with previous findings in other epithelia (Wright & Diamond, 1969; Smulders & Wright, 1971; Dewhurst et al., 1978; Bonting et al., 1980; Steward, 1982). In the case of sucrose, which our studies show not to enter the cellular compartment (Table 3), it is evident that permeation must be via a paracellular route. The same probably holds for mannitol and erythritol. The smaller nonelectrolytes studied can also be expected to have taken the paracellular route, but since they are able, in addition, to enter the cell compartment (Table 3), they may enter the saliva via the transcellular route as well.

The markedly higher value for P observed with ethanediol probably reflects its lipid solubility and suggests that transcellular permeation may be particularly conspicuous for this compound. This particularly high permeability to ethanediol has not been seen in the cat pancreas (Dewhurst et al., 1978) nor in the gallbladders of several species (Diamond & Wright, 1969; Hingson & Diamond, 1972) but it has been observed in both mammalian and amphibian small intestine (Hingson & Diamond, 1972).

The salivary handling of ethanol and antipyrine indicates that these substances are readily able to permeate the epithelium. Their relatively high lipid solubility (Table 1) makes it seem probable that they enter the saliva transcellularly, by-passing the restricted aqueous channels through which the more polar molecules have to pass.

In view of its size and lipid solubility, thiourea ought to have been handled like ethanediol. However, the excretory pattern was quite different (Fig. 4*C*), and the data could not be fitted satisfactorily by Eq. (3). This might be explained by the 'thyroid-like' properties of the duct epithelium of this gland. In certain species, including the rabbit, the intralobular ducts of the mandibular gland are known to trap iodide and to accumulate thiourylene drugs, including thiourea (Connell et al., 1983). The presence of a ductal uptake mechanism for thiourea could thus alter the excretion pattern and make it difficult to interpret in terms of Eq. (3). Alternatively, it may be that the thiourea pattern has been distorted because of its rather high lipid solubility.

Pseudo Solvent Drag

According to the relatively simple analysis of the data applied thus far, the dependence of ϕ on J_v observed with the small polar nonelectrolytes reveals a significant contribution from solvent drag; that is to say, a coupling of solute flux to water flow caused by a frictional interaction between solute and water sharing a common pathway through the

tissue. If this is correct, the dependence of $1 - \sigma$ on solute radius will provide information about the size of the channels through which the secreted fluid is driven.

Before drawing such conclusions, however, it is essential to consider an alternative explanation. Barry and Diamond (1984) have proposed that flow-patterns suggestive of solvent drag may be generated by a mechanism involving diffusion alone; they call the phenomenon 'pseudo solvent drag'. Their suggestion is that in unstirred regions adjacent to a barrier through which water flows, and where $1 - \sigma < 1$, solute accumulation and/or depletion will enhance the solute concentration gradient across that barrier. This in turn will elevate the diffusive solute flux through the barrier to an extent that will vary with J_v in a fashion suggestive of solvent drag.

The geometry of the endpiece epithelium will inevitably favor the occurrence of such a phenomenon: the long narrow intercellular spaces into which water flows will acquire an elevated nonelectrolyte concentration if $1 - \sigma < 1$. This will be more marked at high secretory rates, and diffusive flow through the epithelium will thus increase with J_v. The model ignores the presence of unstirred layers in the cytosol compartment, which, though clearly present, would have only a minimal effect in comparison with the long narrow intercellular spaces. The critical question therefore is: how much of what appears to be solvent drag can be explained by pseudo solvent drag?

To answer this question, a simple geometrical model of the mandibular gland endpiece (described in outline in the Appendix) may be used to generate nonelectrolyte flow curves that take into account these unstirred-layer effects. For example, suppose that water flow across the epithelium is entirely transcellular and that the nonelectrolyte in question enters the saliva by diffusion alone. By setting the diffusive permeability parameters in the model so that the predicted flow curves fit the experimental data points at low flow rates (where diffusive flow will in any case predominate), it is possible to see whether or not the unstirred layer phenomenon can generate an elevated plateau of ϕ which might be mistaken for true solvent drag.

Using urea as an example, Fig. 5 shows the experimental data from a single representative experiment and flow curves that were generated by the model. Using an estimate of the epithelial secretory area of the gland (calculated as described in the Appendix), the model predicts negligible pseudo solvent drag (curve *a*). This is because, even at the highest secretory rates, the fluid velocities through the unstirred regions of the epithelium are not large enough to cause a substantial accumulation of non-

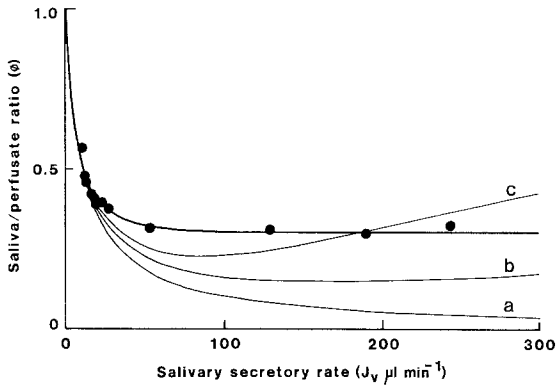

Fig. 5. Flow curves for urea generated for a geometrical endpiece model, compared with data (●) from a single experiment. Curve *a* assumes an epithelial basal surface area of 910 cm^2, and this was reduced to 2.3 cm^2 and 0.91 cm^2 for curves *b* and *c*, respectively. *P* values have been adjusted to give a good fit to the data in the range 0 to 20 μl min^{-1}. The bold curve shows the best-fitting function of the form given by Eq. (3) where $P = 5.96$ mm^3 min^{-1} and $1 - \sigma = 0.302$

electrolyte. In the event of the true epithelial area being 400 times less than our estimate, and the fluid velocities correspondingly greater, pseudo solvent drag would, however, be expected to be more significant and to give rise to a low but relatively flat plateau (curve *b*). When we reduce the area estimate further in an attempt to match the predicted curve to the data, the curve fails to remain flat (curve *c*). Indeed, it is a general property of pseudo solvent drag that, above a certain flow rate, ϕ begins to rise with J_v in a way that was not observed in any of our experiments. It appears impossible, therefore, that pseudo solvent drag alone could have generated the high, flat plateau seen in the urea data. Some contribution from pseudo solvent drag is, however, inevitable, although our calculations show that at most it will be small.

The Nature of the Fluid Channels

While the evidence for solvent drag of small polar nonelectrolytes during secretion seems strong, the route by which they penetrate the endpiece epithelium remains uncertain. The identity of this route is of considerable importance because the dominant contribution of solvent drag suggests that this is also the route taken by some at least of the secreted water. Although the results presented here do not allow us to distinguish between transcellular and paracellular routes, they do provide information about the size of the channels in which solvent drag occurs and through which the secreted water is presumably driven. If the channels are simple cylindri-

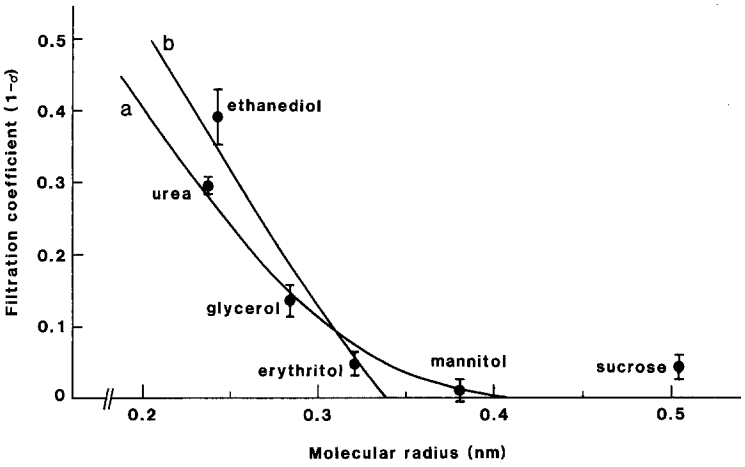

Fig. 6. The relation between $1 - \sigma$ and molecular radius. Experimental data for six nonelectrolytes are means ± SEM where $n = 5$ to 7. Curve *a* is the relation predicted for a population of cylindrical pores (Haberman & Sayre, 1958) of radius 0.42 nm, and curve *b* for a system of parallel-sided slits (Happel & Brenner, 1965) of half-width 0.34 nm

cal pores or parallel-sided slits, hydrodynamic theory may be used to interpret the dependence of $1 - \sigma$ on molecular radius (Renkin & Curry, 1979). If we assume that all the secreted water passes through the channels, and that the channel population is homogeneous, curves such as those in Fig. 6 can be plotted. Either pores of 0.42-nm radius (curve *a*) or slits of 0.34-nm half-width (curve *b*) would account reasonably well for the experimental data. Because, however, the drag factors employed in these calculations are subject to substantial errors as molecular radius approaches channel radius, it would be unwise to conclude more than that the effective channel radius is approximately 0.4 nm.

We thank the U.K. Cystic Fibrosis Trust for initial support of this work and the S.E.R.C. (U.K.) for subsequent support and the award of a Senior Visiting Research Fellowship to J.A.Y.

References

Barry, P.H., Diamond, J.M., 1984. Effects of unstirred layers on membrane phenomena. *Physiol. Rev.* **64:**763–872

Bonting, S.L., Pont, J.J.H.H.M. de, Fleuren-Jakobs, A.M.M., Jansen, J.W.C.M. 1980. The reflexion coefficient as a measure of transepithelial permeability in the isolated rabbit pancreas. *J. Physiol. (London)* **309:**547–555

Burgen, A.S.V. 1956. The secretion of non-electrolytes in the parotid saliva. *J. Cell. Comp. Physiol.* **48:**113–138

Burgen, A.S.V., Emmelin, N.G. 1961. Physiology of the Salivary Glands. Arnold, London

Case, R.M., Conigrave, A.D., Novak, I., Young, J.A. 1980. Electrolyte and protein secretion by the perfused rabbit mandibular gland stimulated with acetylcholine or catecholamines. *J. Physiol. (London)* **300:**467–487

Case, R.M., Hunter, M., Steward, M.C., Young, J.A. 1983. Non-electrolyte transport by the isolated rabbit mandibular salivary gland. *J. Physiol. (London)* **342:**83–84P

Collander, R. 1954. The permeability of *Nitella* cells to non-electrolytes. *Physiol. Plant.* **7:**420–445

Connell, J.M., McCruden, D.C., Small, M., Ferguson, M.M., Alexander, W.D. 1983. Accumulation of thiourylene antithyroid drugs in mouse salivary glands. *J. Endocrinol.* **96:**91–96

Cornish-Bowden, A. 1976. Principles of Enzyme Kinetics. Butterworths, London and Boston

Dewhurst, D.G., Hadi, N.A., Hutson, D., Scratcherd, T. 1978. The permeability of the secretin stimulated exocrine pancreas to non-electrolytes. *J. Physiol. (London)* **277:**103–114

Diamond, J.M., Wright, E.M. 1969. Molecular forces governing non-electrolyte permeation through cell membranes. *Proc. R. Soc. London B* **172:**273–316

Haberman, W.L., Sayre, R.M. 1958. Motion of rigid and fluid spheres in stationary and moving liquids inside cylindrical tubes. *In:* David Taylor Model Basin Hydromechanics Lab. R. & D. Report No. 1143. U.S. Dept. of the Navy. Cited by Renkin and Curry (1979)

Happel, J., Brenner, H. 1965. Low Reynolds Number Hydrodynamics. Prentice-Hall, Englewood Cliffs, N.J.

Hingson, D.J., Diamond, J.M. 1972. Comparison of nonelectrolyte permeability patterns in several epithelia. *J. Membrane Biol.* **10:**93–135

Kedem, O., Katchalsky, A. 1958. Thermodynamic analysis of the permeability of biological membranes to non-electrolytes. *Biochim. Biophys. Acta* **27:**229–246

Longsworth, L.G. 1953. Diffusion measurements, at 25°C, of aqueous solutions of amino acids, peptides and sugars. *J. Am. Chem. Soc.* **75:**5705–5709

Mangos, J.A., Maragos, N., McSherry, N.R. 1973. Micropuncture and microperfusion study of glucose excretion in rat parotid saliva. *Am. J. Physiol.* **224:**1260–1264

Mangos, J.A., McSherry, N.R. 1970. Micropuncture study of urea excretion in parotid saliva of the rat. *Am. J. Physiol.* **218:**1329–1332

Middleton, E. 1977. The molecular configuration of inulin: Implications for ultrafiltration theory and glomerular permeability. *J. Membrane Biol.* **34:**93–101

Patlak, C.S., Goldstein, D.A., Hoffman, J.F. 1963. The flow of solute and solvent across a two-membrane system. *J. Theor. Biol.* **5:**426–442

Phelps, C.F. 1965. The physical properties of inulin solutions. *Biochem. J.* **95:**41–47

Potter, A.J., Steward, M.C., Case, R.M. 1984. Effect of acetylcholine concentration on non-electrolyte secretion by the perfused rabbit mandibular salivary gland. *In:* Secretion:

Mechanisms and Control. R.M. Case, J.M. Lingard and J.A. Young, editors. pp. 137–141. Manchester University Press, Manchester, and Dover, New Hampshire

Renkin, E.M., Curry, F.E. 1979. Transport of water and solutes across capillary endothelium. *In:* Membrane Transport in Biology, Vol. IVA. G. Giebisch, D.C. Tosteson and H.H. Ussing, editors. pp. 1–46. Springer, Berlin, Heidelberg and New York

Schultz, S.G., Solomon, A.K. 1961. Determination of the effective hydrodynamic radii of small molecules by viscometry. *J. Gen. Physiol.* **44:**1189–1199

Smulders, A.P., Wright, E.M. 1971. The magnitude of nonelectrolyte selectivity in the gallbladder epithelium. *J. Membrane Biol.* **5:**297–318

Stein, W.D. 1967. The Movement of Molecules across Cell Membranes. Academic, New York and London

Steward, M.C. 1982. Paracellular non-electrolyte permeation during fluid transport across rabbit gall-bladder epithelium. *J. Physiol. (London)* **322:**419–439

Takai, N., Yoshida, Y., Kakudo, Y. 1983. Secretion and reabsorption of glucose in rat submandibular saliva. *J. Dent. Res.* **62:**1022–1025

Welch, R.M., Angelis, R.L. de, Wingfield, M., Farmer, T.W. 1975. Elimination of antipyrine from saliva as a measure of metabolism in man. *Clin. Pharmacol. Ther.* **18:**249–258

Wright, E.M., Diamond, J.M. 1969. Patterns of non-electrolyte permeability. *Proc. R. Soc. London B* **172:**227–271

Wright, E.M., Pietras, R.J. 1974. Routes of nonelectrolyte permeation across epithelial membranes. *J. Membrane Biol.* **17:**293–312

Young, J.A., Lennep, E.W. van 1978. The Morphology of Salivary Glands. Academic, London

Young, J.A., Lennep, E.W. van 1979. Transport in salivary and salt glands. *In:* Membrane Transport in Biology, Vol. IVB. G. Giebisch, D.C. Tosteson and H.H. Ussing, editors. pp. 563–692. Springer, Berlin, Heidelberg and New York

Received 16 August 1984; revised 13 November 1984

Appendix

Computation of Nonelectrolyte Flow Curves using a Geometrical Model of the Rabbit Mandibular Gland Epithelium

The following paragraphs outline the main features of a model that has been used to evaluate the contribution of pseudo solvent drag to the nonelectrolyte flow curves.

Geometry

The secretory endpieces of the rabbit mandibular gland are approximated by the simplified geometrical model shown in Fig. 7. The principal unstirred regions are (a) the intercellular spaces (interspaces) which taper from a width of 2 μm at the basal end to 5 nm at the luminal end, and (b) a thin layer of fluid 4 μm thick covering the basal membrane of the epithelial cells. The value of 4 μm is somewhat arbitrary but, because the calculated unstirred layer effects there are so small compared with the effects in the interspaces, even increasing the figure by a factor of 10 would make virtually no difference to our conclusions. The effects of unstirred layers within the cell on our analysis can also be expected to be small and thus, for simplicity, are neglected in this model.

Since the volume of each endpiece as defined in Fig. 7 is 1.2×10^5 μm^3, and the total volume of a typical gland is 1 cm^3 (the endpieces occupying approximately 85% of the total, Young & van Lennep, 1978), it can be calculated that each gland contains approximately 7×10^6 endpieces. The external (basal) surface of each endpiece is 1.3×10^4 μm^2 so the total basal endpiece surface area per gland is around 910 cm^2.

Volume Flow

For the purposes of this study, the secretory water flow into each endpiece cell is taken to be uniformly distributed over the basal and lateral membranes with no fluid movement through the junctional complexes. The volume flux per unit area across the basolateral membrane is thus

$$J_v^C = \frac{J_v}{A^B + A^L} \tag{A1}$$

where J_v is the total volume flow per gland, i.e. the secretory rate, and A^B and A^L are the basal and lateral membrane areas (per gland). Across the basal membrane the volume flow (per gland) will thus be

$$J_v^B = J_v^C A^B. \tag{A2}$$

The volume flow along the interspace declines from an initial value of $J_v - J_v^B$ to zero at the luminal end according to

$$\frac{dJ_v^{IS}}{dx} = -J_v^C L(x) \tag{A3}$$

where $L(x)$ is the cell perimeter at distance x from the mouth of the interspace.

Nonelectrolyte Tracer Flow

For the purposes of simulating pseudo solvent drag, the nonelectrolyte is considered to cross the junctional and cell membrane barriers by diffusion alone.

The nonelectrolyte flux across the basal membrane and its associated unstirred layer will be

$$J_n^B = P^C A^B \{C^M - C^S\} \tag{A4}$$

where P^C is the transcellular nonelectrolyte permeability per unit area of basolateral membrane (the sum by reciprocals of the

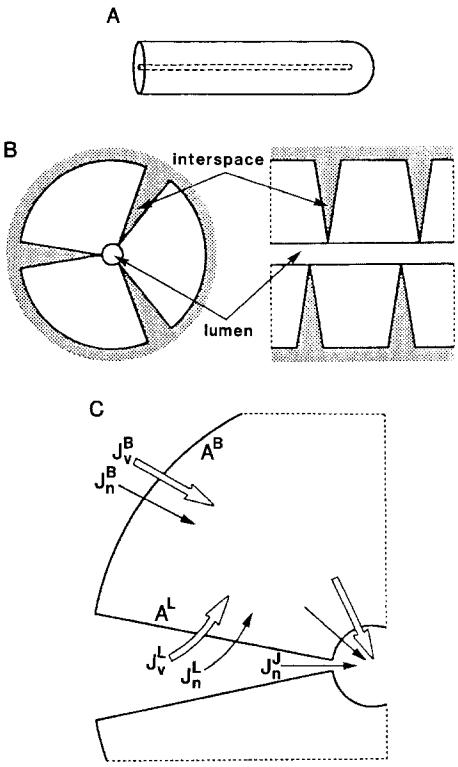

Fig. 7. Geometry of the mandibular gland endpiece model. *A*. Each endpiece is approximated by a cylindrical tubule 180 μm in length with an outside diameter of 40 μm and a luminal diameter of 2 μm terminated at one end by a hemisphere. *B*. Transverse and longitudinal sections of the endpiece. At any point, three cells surround the lumen, each having a radial height of 19 μm and a length of 40 μm along the tubule axis. Unstirred regions where nonelectrolyte accumulation might lead to pseudo solvent drag are shown shaded. *C*. Expanded tranverse section (not to scale) showing routes of nonelectrolyte flow (thin arrows) and volume flow (thick arrows), and the interspace geometry chosen for the present study

basolateral and apical permeabilities). C^M, the elevated nonelectrolyte concentration in the unstirred layer at the basal membrane surface, is calculated by integrating the nonelectrolyte flow equation,

$$D_o \frac{dC}{dx} = J_v^C C(x) - \frac{J_n^B}{A^B} \tag{A5}$$

where D_o is the free-solution diffusion coefficient, across the thickness δ^B of the unstirred layer. The resulting equation for nonelectrolyte flow across the basal membrane is

$$J_n^B = \frac{P^C A^B \{C^P \exp(J_n^C \delta^B / D_o) - C^S\}}{1 - P^C \{1 - \exp(J_n^C \delta^B / D_o)\} / J_n^C}. \tag{A6}$$

The nonelectrolyte flow along the interspace will decline with x according to

$$\frac{dJ_n^{IS}}{dx} = -P^C L(x)\{C(x) - C^S\} \tag{A7}$$

where $C(x)$ is the concentration at x. And through the junction

$$J_n^J = P^J\{C(a) - C^S\} \tag{A8}$$

where P^J is the junctional nonelectrolyte permeability (per gland) and $C(a)$ is the concentration at the luminal end of the interspace.

Computation of C^S

In the steady state, the nonelectrolyte tracer flux along the interspace (J_n^{IS}) has to obey, not only Eq. (A7) but also the diffusion-convection equation for longitudinal solute flow:

$$J_n^{IS}(x) = J_v^{IS}(x) \cdot C(x) - D_o A(x) \frac{dC}{dx} \tag{A9}$$

where $A(x)$ is the cross-sectional area of the interspace (per gland) at x. Combining Eqs. (A7) and (A9) we have

$$-D_o A(x) \frac{d^2C}{dx^2} + \left\{J_v^{IS}(x) - D_o \frac{dA}{dx}\right\} \cdot \frac{dC}{dx} + \left\{\frac{dJ_v^{IS}}{dx} + P^C L(x)\right\} \cdot C(x) - P^C L(x) C^S = 0. \tag{A10}$$

Using the geometrical model of Fig. 7, Eq. (A10) is solved for $C(x)$ by numerical integration (using routine D02CAF of the NAG library) starting at $x = 0$, where the boundary conditions are

$$C = C^P = 1 \tag{A11}$$

$$\frac{dC}{dx} = \frac{C^P(J_v - J_n^B) - (J_n - J_n^B)}{D_o A(0)}. \tag{A12}$$

Steady-state solutions of Eq. (A10) which also satisfy Eq. (A8) are found by iteration, and values of $\phi = C^S/C^P$ are calculated for different volume flow rates within the physiological range (0 to 300 μl/min).